J Mater Sci (2009) 44:5143–5148
DOI 10.1007/s10853-009-3512-x

FERROELECTRICS

Room temperature magnetic exchange coupling in multiferroic $BaTiO_3/CoFe_2O_4$ magnetoelectric superlattice

J. X. Zhang · J. Y. Dai · W. Lu · H. L. W. Chan

Received: 16 March 2009 / Accepted: 22 April 2009 / Published online: 6 May 2009

Abstract Multiferroic $BaTiO_3/CoFe_2O_4$ superlattice films are deposited by laser molecular beam epitaxy. The film growth modes are studied by in situ reflection high energy electron diffraction and the film structures are revealed by high resolution transmission electron microscopy study. Ferroelectric switching behavior was studied by piezoresponse force microscopy, and it shows that good ferroelectricity was retained in the superlattice. Such a multiferroic superlattice also shows a magnetic exchange coupling under room temperature. Detailed analysis reveals that different growth modes and the substrate strain effect may be responsible for the magnetic exchange coupling.

Introduction

Over the last few years, magnetoelectric (ME) nanocomposites have received a lot of interest due to their potential applications on many multifunctional devices such as sensor, non-volatile memory etc. [1]. Due to the reason that single-phase multiferroic materials are rare and their ME coupling response is weak, [2] the magnetic field induced electric polarization and electric field induced magnetization in ferroelectric/ferromagnetic nanocomposite are being extensively studied [3–6]. Traditional ME effect in composite system originates from the strain coupling around the interface of ferroelectric and ferromagnetic components; therefore, there has been a great effort to optimize the growth and study of the coupling mechanism of ferroelectric and magnetic nanocomposite thin films.

Besides traditional ME effect, it is interesting to notice that enhanced polarization has been observed in ferroelectric superlattice [7]. Some theoretical argument [8] supports the point that it is the electric mechanism not the traditional strain coupling at the interface of ferroelectric/ferromagnetic that creates the ME effect. Yang et al. [9] report that the ferroelectricity is induced by superlattice structure in $BiMnO_3$ crystal. This provides useful guideline for new materials design. Especially, it will show novel ferroelectric and magnetic behavior when the size of ferroelectric and magnetic phase reduces to nano or atomic scale [10, 11]. Therefore, it becomes significant to study the multiferroic properties and control the growth of ME nanocomposite [12]. At the same time, interlayer exchange coupling in magnetic tunnel junctions composed of two ferromagnetic layers separated by an insulator layer [13] has attracted a great deal of attention due to their application in magnetic read heads, magnetic sensors, etc.

In this article, highly epitaxial multiferroic superlattice $CoFe_2O_4$ (CFO)/$BaTiO_3$ (BTO) nanocomposites on $SrTiO_3$ (STO) and MgO substrates were deposited using laser molecular beam epitaxy (MBE) with in situ monitoring of the growth mode by reflected high energy electron diffraction (RHEED). There have been some reports about the strain-induced electric property in CFO/BTO multilayers [14], but the magnetic property has not been well studied in the superlattice structure. The magnetic interlayer exchange coupling effect under room temperature is first reported in this ferroelectric/magnetic superlattice with ferroelectric interlayer, which may provide a new route for the introduction of the ME nanocomposite into spintronics and multiferroic tunneling junction.

J. X. Zhang · J. Y. Dai (✉) · W. Lu · H. L. W. Chan (✉)
Department of Applied Physics, The Hong Kong Polytechnic University, Hung Hom, Kowloon, Hong Kong
e-mail: apdaijy@inet.polyu.edu.hk

H. L. W. Chan
e-mail: apahlcha@inet.polyu.edu.hk

Experimental details

A series of BTO/CFO superlattice with different periodicity and thickness were deposited on (001)-oriented Nb-doped $SrTiO_3$ (STO) and MgO substrates by laser-MBE, using a KrF excimer laser of 248 nm in wavelength, 1 Hz in repetition rate, and 2.50 J/cm^2 in laser energy density. The stoichiometric targets of CFO and BTO were prepared through a standard solid reaction sintering processing. The substrates were cleaned by acetone, ethanol, and DI water bath routinely and annealed in situ for 30 min at 800 °C. The working pressure used for depositing the superlattice was 5×10^{-4} Pa, and substrate temperature was 700 °C. The films were in situ annealed for half-an-hour and cooled down at 1 atm oxygen pressure in order to compensate the oxygen vacancy during the growth. The first and ending layer were always controlled as BTO to eliminate the space charge in the interface of electrode and low resistance CFO during electrical characterization. RHEED was employed to confirm the epitaxial growth and establish the growth mode. In order to carry out electrical property measurements, Pt dot electrode with a diameter of 0.2 mm was deposited on the top surface of the thin films by PLD. The ferroelectric hysteresis loops of the BTO/CFO superlattice were measured using a ferroelectric tester (TF Analyzer 2000, aixACCT) at 1 kHz. Spectroscopic dielectric behavior of the superlattice was measured by an impedance analyzer (Agilent 4294A).

Results and discussion

The epitaxy and growth mode of BTO/CFO (indicated by B and C, respectively) superlattice were studied by RHEED recorded during the film deposition in [100] azimuth of the substrates (shown in Fig. 1). The patterns for STO (Fig. 1a) and MgO (Fig. 1d) substrates after in situ annealing, as well as BTO on STO (Fig. 1b) show vertical lattice rods and sharp Kikuchi lines, suggesting well ordered and smooth surface with Frank-van der Merwe growth mode (layer-by-layer). However, the initial CFO layer with a thickness of 2 nm grown on BTO/STO (Fig. 1c) shows spotty pattern, suggesting Volmer–Weber (island) growth mode due to the lower mobility of adatoms under large lattice mismatch (~7.4%). The BTO on MgO substrate (Fig. 1e) and the CFO on BTO/MgO (Fig. 1f) also show the island growth mode. It is evident that the epitaxial nature is strongly dependent on the lattice mismatch and the crystal structures. Two-dimensional layer-by-layer growth mode appears in BTO on STO substrate due to their small lattice mismatch. It is worth noting that the growth mode and the lattice structure are different between the first and the rest CFO layers on STO substrate according to the RHEED patterns shown in Fig. 2, which is the result of the strain release of the second CFO layer on top of the B/C/B/STO stacks. While the first CFO layer grown on top of BTO/STO suffers the total in-plane compressive strain because of the large lattice mismatch (~7.4%), and therefore, the spotty pattern can be seen. Observed from the RHEED patterns, the growth mode of CFO was kept the same after the deposition of second CFO layer through the whole superlattice, where the streaky plus spot pattern indicate the Stranski–Krastanov and the strain relaxation in the following CFO.

The morphology and microstructure of the superlattice were studied by cross-sectional high-resolution transmission electron microscopy (HRTEM, using a JEOL 2010 electron microscope operated at 200 kV). Figure 3a, b shows the cross-sectional morphologies of B/C/B/C/B superlattice on [001] oriented STO and MgO substrates, respectively, with high-quality epitaxial growth relationship and sharp interfacial structure between superlattice

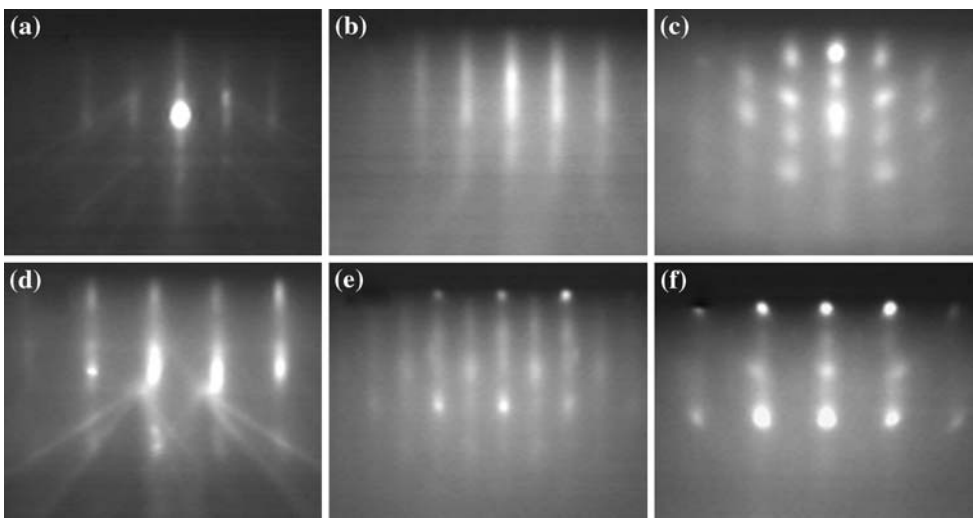

Fig. 1 RHEED pattern images of **a** UHV annealed STO substrate, **b** after 2.5 nm BTO grown on STO, **c** after 2 nm CFO growth on BTO/STO, **d** UHV annealed MgO substrate, **e** after 2.5 nm BTO growth on MgO, and **f** after 2 nm CFO growth on BTO/MgO. The images were recorded in [100] azimuth

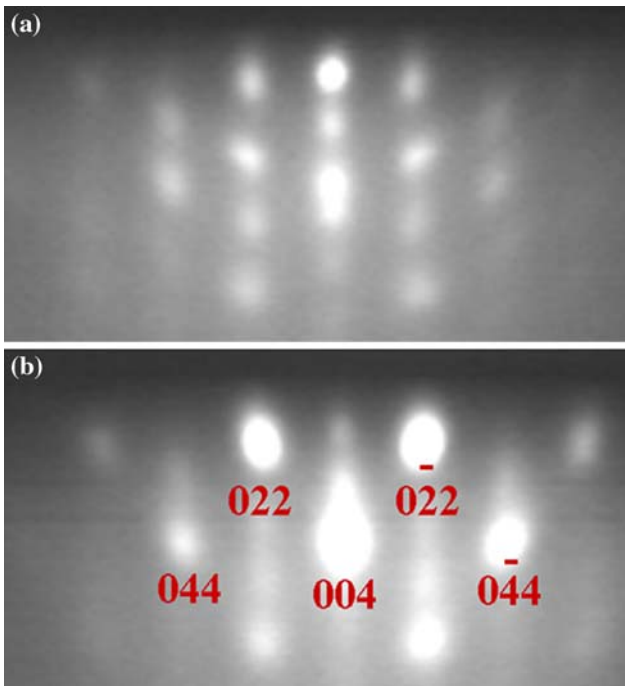

Fig. 2 RHEED pattern images of **a** the first CFO layer grown on BTO/STO and **b** the following CFO layers grown on BTO/CFO/BTO/STO. The images were recorded in [100] azimuth

and the substrates, which is in good agreement with RHEED patterns. The BTO/CFO superlattice is perfectly oriented and the epitaxial crystalline structure shows the orientation relations of BTO (00*l*)//CFO (00*l*)//STO (00*l*). In the superlattice, the BTO was controlled as 5 unit cells, and CFO was controlled as 2 unit cells. Clear interfacial structures between CFO and BTO, BTO and STO, and BTO and MgO are shown in the inset of Fig. 3. There is no obvious inter-diffusion at the interface.

The dielectric and ferroelectric properties along the thickness direction (ε_{33}) and (P_3) with the conductive Nb:STO bottom electrode substrates were measured. Good ferroelectric property was verified by the typical ferroelectric hysteresis loops, shown in Fig. 4a. Tested under a field with a maximum strength of 200 MV/m, the saturated loop was observed with a remnant polarization (P_r) of 2.1 μC/cm^2 and coercive field (E_c) of 75 MV/m. The remnant polarization is lower than the value (25 μC/cm^2) of pure BTO single crystal [15], but close to the polarization of 3.0 and 5.4 μC/cm^2 in $BaTiO_3/SrTiO_3/CaTiO_3$ asymmetric ferroelectric superlattice [7] and larger than the polarization of BTO/STO superlattice reported before [16]. That means good ferroelectricity can be obtained from ferroelectric/dielectric superlattice not only in perovskite/perovskite systems, but also the perovskite/spinel heterostructure. The decreased polarization in the present BTO/CFO superlattice mainly originated from the effect of the "dilution" of the ferroelectric material (BTO) in a non-ferroelectric matrix (CFO), which can be illustrated by the formula:

$$P_s = \frac{P_B}{1 + \frac{\phi_c}{\phi_B} \cdot \frac{\varepsilon_B}{\varepsilon_c}},$$

where P_s and P_B are the spontaneous polarizations of the superlattice and BTO, respectively; ϕ_c and ϕ_B are the volume fractions of CFO and BTO in the superlattice, and ε_B and ε_c represent the dielectric constants of BTO and CFO, respectively. Another important factor that breaks the ferroelectric order is the insertion of low dielectric constant layer of CFO. Therefore, the observed polarization in superlattice is lower than the calculated data (3.1 μC/cm^2) due to the contribution of leakage from CFO. Spectroscopic dielectric behaviors of the superlattice were shown in Fig. 4b. In the superlattice capacitor, the dielectric constant shows weak frequency-dependent nature and is lower than the single phase BTO ($\varepsilon = 160$) due to the existence of CFO layer ($\varepsilon = 10$). From the dielectric spectroscopy, we cannot see the space charge induced relaxation at ~10–100-kHz region, which is obvious in

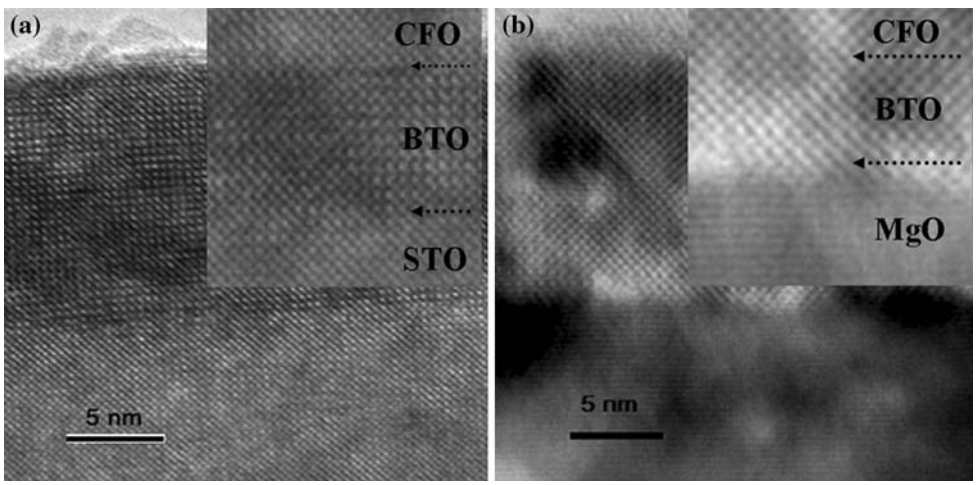

Fig. 3 HRTEM image of BTO/CFO superlattice grow on **a** STO and **b** MgO substrates. The insets show the clear interface structure

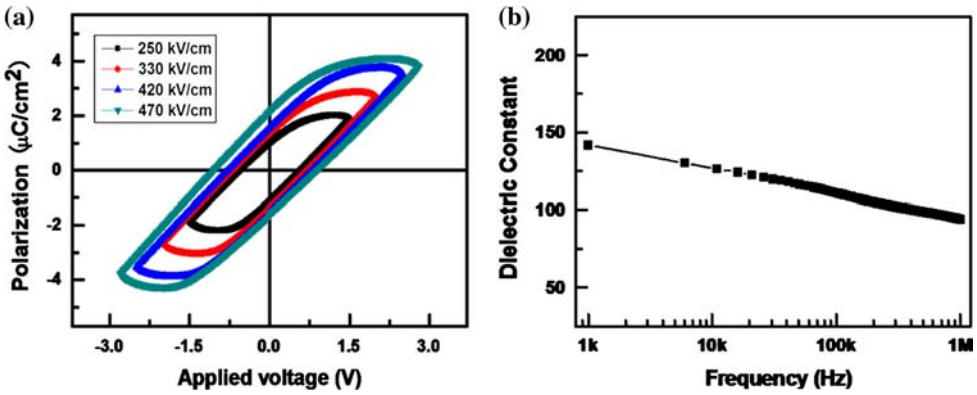

Fig. 4 **a** Ferroelectric hysteresis loops and **b** spectroscopic dielectric constant of BTO/CFO superlattice capacitor

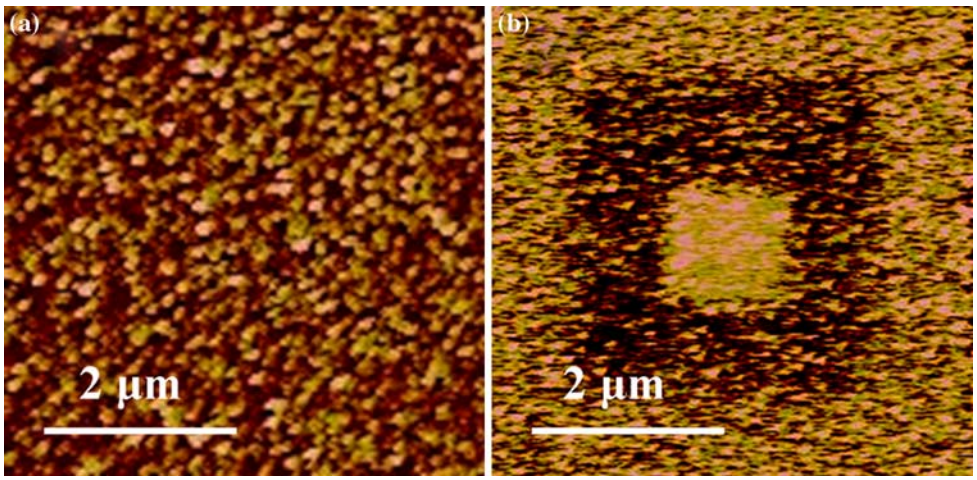

Fig. 5 **a** The AFM image, **b** PFM image after we poled the sample by −2.5 V (*dark region*) and +2.5 V voltage (*bright region*)

PZT/CFO multilayer deposited by PLD [17]. This can be further explained by the clear and well-controlled interface between BTO and CFO without interdiffusion and reaction.

Piezoresponse force microscopy of the superlattice was acquired by the multimode atomic force microscope (Nanoscope IV, Digital Instruments). In our experiments, a Pt-coated conductive probe was used for the contact mode piezoresponse force microscopy (PFM) imaging. Figure 5a shows the topography images, while Fig. 5b shows the corresponding out-of-plane PFM image of the superlattice. A voltage of 1 V (peak-to-peak) with 11 kHz was applied to the bottom electrode of the sample, while the tip was electrically grounded. From the out-of-plane PFM image, we can see that the spontaneous polarization direction in the superlattice was pointing down because of the build-in electric field in the interface of Nb:STO substrate and the superlattice film. We switched the sample by scanning an area in contact mode with a conductive probe biased at −2.5 V over 3 × 3 μm^2, and then the sample was switched back with the probe biased at +2.5 V over the central area of 1 × 1 μm^2. A clear domain switching process can be observed in the PFM image. The dark region indicates the area that was switched at a negative electric field and the central bright region indicates the area that was switched at a positive electric field. This domain switching effect can further prove the good ferroelectric property in the local area of the superlattice.

The multiferroic nature of the nanocomposite films can be illustrated by the coexistence of good ferroelectric and ferro/ferrimagnetic behaviors at room temperature. The magnetic hysteresis loops of the BTO/CFO superlattice were systematically characterized by a vibrating sample magnetometer (VSM, Lakeshore, Model 7300 series). The volume of the CFO component was calculated by the area of substrate times the thickness of the CFO layers. All of curves were measured under room temperature. The typical saturated magnetic hysteresis loops of the BTO/CFO superlattice (B/C/B/C/B) grown on STO and MgO substrates are shown in Fig. 6. Both of the measurements were performed with the magnetic field parallel to the film planes.

The saturated magnetization of superlattice grown on STO is 350 emu/cm^3, which is much higher than the one on MgO and very close to the value of bulk CFO. The coercive fields of the superlattice are 75 and 50 Oe for the superlattice on STO and MgO substrates, respectively, shown in the inset of Fig. 6. The dramatically decrease of the coercive field and the remnant magnetization (comparing to

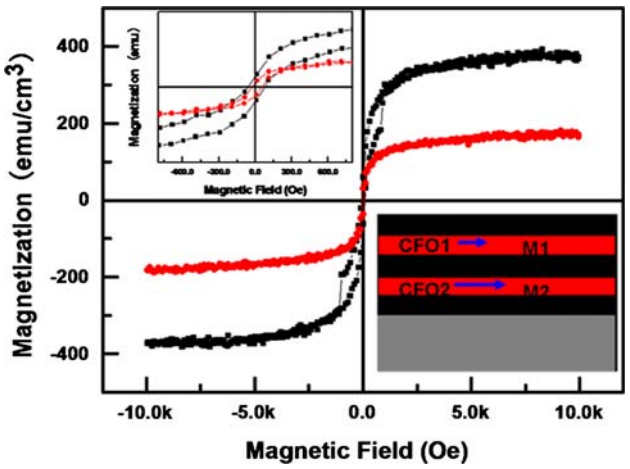

Fig. 6 Magnetic hysteresis loops of superlattice (BCBCB) grown on STO (*higher curve*) and MgO (*lower curve*) substrates. The inset graph shows the magnified curve

100 nm CFO epitaxial film [18]) is attributed to the superparamagnetic nature of nanoscale CFO, especially when the size reduces below 10 nm [19]. The magnetization of superlattice on STO is larger than the value of superlattice grown on MgO. This phenomenon can also be observed in the pure CFO epitaxial thin film (100 nm) deposited on STO and MgO substrates, as shown in Fig. 7. The magnetostrictive nature of CFO may be responsible for the difference of in-plane magnetization in both samples, which is discussed elsewhere [20]. According to a general Le Chatelier's principle [21], it is also well known that the effect of stress on magnetization, coercive field and permeability is mainly originated from the magnetostrictive nature of the materials. If a material has a positive magnetostrictive coefficient (λ), it will elongate when magnetized; reversely, its magnetization will increase under a tensile stress and will decrease under a compressive stress. In the contrary, if a material has a negative magnetostrictive

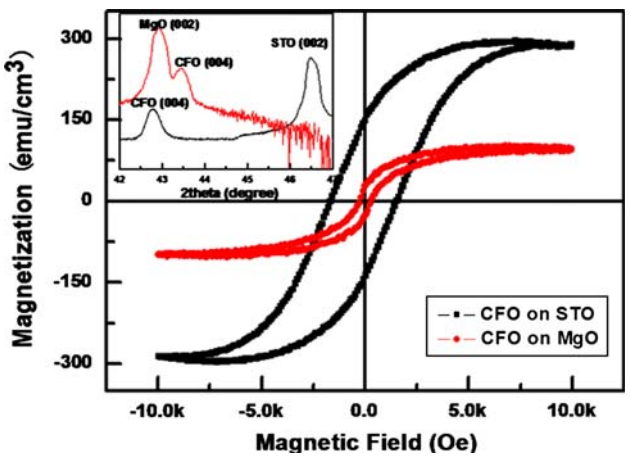

Fig. 7 Magnetic hysteresis loops of CFO epitaxial films grown on STO and MgO substrates. The inset shows the XRD peaks indicating the different lattice strains

coefficient, its magnetization increases when a compressive stress is applied.

For the superlattice B/C/B/C/B on STO substrate, obvious magnetic exchange interaction happens via the ferroelectric BTO spacer layer. This kind of interlayer magnetic coupling effect can usually be seen in metallic thin films [22] and also MgO interlayer in oxide system [23]. In this case, 2.5-nm thick ferroelectric BTO ($\sim$6 unit cells) acts as the insulating layer between two ultrafine CFO phases. It can be roughly understood that different growth modes of the two CFO layers, which is already addressed in the discussion of RHEED patterns, may be one of the possible origins that produce different magnetic state (magnetization and coercive field). Via the BTO space layer, the magnetic exchange coupling happens in the superlattice grown on STO, but not on MgO substrate. The magnetic hysteresis loop of superlattice grown on STO can be understood as the combination of two loops originated from the two CFO layers with different magnetic states. Lower and upper CFO layers possess different magnetization and coercive field because they have different in-plane strains and growth modes. The two CFO layers can be considered as two single CFO films suffered from different strains as the illustration of Fig. 7 at the extreme condition. The magnetic hysteresis loop in superlattice can also be considered as the combination of the two curves like the loops in Fig. 7.

When we increase the thickness of the superlattice to $\sim$52 nm with 5 unit cells (10 B_5C_5) and 10 unit cells (5 $B_{10}C_{10}$) for each layer, respectively, the magnetic exchange coupling disappear and the magnetization is also decreased compared to the one in 12.5 nm superlattice, as shown in Fig. 8. After the deposition of second CFO layer, the growth mode becomes the same in the following CFO according to the RHEED patterns. Therefore, the following

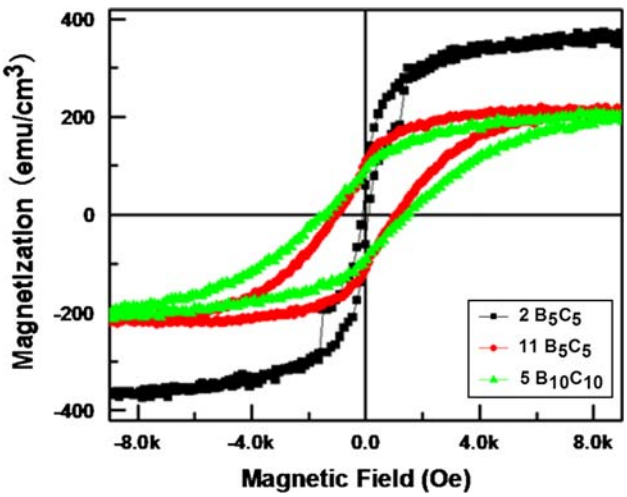

Fig. 8 Magnetic hysteresis loops of BTO/CFO superlattice grown on STO substrates with different thickness

CFO layers suffer the similar in-plane strain and will possess the same magnetic state. The magnetic exchange coupling in the first two layers was "diluted" by the following growth of CFO in the superlattice. The released in-plane compressive strain induces the decrease of the magnetization of superlattice as discussed above. This compressed magnetic exchange coupling and magnetization can also be found in the superlattice with an increased unit cells in each layer. Apart from the "dilution" of the difference of magnetic state between each CFO layer, inhibiting exchange coupling between CFO, the in-plane compressive strain will be further relaxed with the increase of thickness in each CFO layer, which explain the further increase of coercive field and decrease of the magnetization.

Conclusion

We have deposited the BTO/CFO superlattice with in situ monitoring of the growth mode by laser-MBE and RHEED. Good ferroelectric and dielectric properties were retained in the multiferroic nanocomposite. Magnetic exchange coupling was first observed in the superlattice B/C/B/C/B/STO structure with ferroelectric materials as the interlayer under room temperature. This magnetic exchange coupling in ferroelectric/magnetic superlattice can introduce further potential possibilities for manipulating the magnetic behaviors of the multiferroic system with more freedom.

Acknowledgement The authors would like to thank the financial support from the collaboration project grant between the Hong Kong Polytechnic University and Beijing Institute of Technology (No. 1-BB84). J. Y. Dai is grateful to the financial support from the Hong Kong GRF grant: PolyU 5005/08P.

References

1. Spaldin NA, Fiebig M (2005) Science 309:391
2. Wang J, Neaton JB, Zheng H, Nagarajan V, Ogale SB, Liu B, Viehland D, Vaithyanathan V, Schlom DG, Waghmare UV, Spaldin NA, Rabe KM, Wuttig M, Ramesh R (2003) Science 299:1719
3. Zavaliche F, Zheng H, Mohaddes-Ardabili L, Yang SY, Zhan Q, Shafer P, Reilly E, Chopdekar R, Jia Y, Wright P, Schlom DG, Suzuki Y, Ramesh R (2005) Nano Lett 5:1793
4. Chaudhuri AR, Ranjith R, Krupanidhi SB, Mangalam RVK, Sundaresan A (2007) Appl Phys Lett 90:122902
5. Zhang JX, Dai JY, Lu W, Chan HLW, Wu B, Li DX (2008) J Phys D Appl Phys 41:235405
6. Ren SQ, Weng LQ, Song S-H, Li F, Wan JG, Zeng M (2005) J Mater Sci 40:4375. doi:10.1007/s10853-006-7897-5
7. Lee HN, Christen HM, Chisholm MF, Rouleau CM, Lowndes DH (2005) Nature 433:395
8. Stengel M, Spaldin NA (2006) Nature 443:679
9. Yang H, Chi ZH, Jiang JL, Feng WJ, Dai JF, Jin CQ, Yu RC (2008) J Mater Sci 43:3604. doi:10.1007/s10853-008-2571-8
10. Fong DD, Stephenson GB, Streiffer SK, Eastman JA, Auciello O, Fuoss PH, Thompson C (2004) Science 304:1650
11. Voogt FC, Palstra TTM, Niesen L, Rogojanu OC, James MA, Hibma T (1998) Phys Rev B 57:R8107
12. Ramesh R, Spaldin N (2007) Nature Mater 6:21
13. van der Heijden PAA, Bloemen PJH, Metselaar JM, Wolf RM, Gaines JM, van Eemeren JTWM, van der Zaag PJ, de Jonge WJM (1997) Phys Rev B 55:11569
14. Huang W, Zhu J, Zeng HZ, Wei XH, Zhang Y, Li YR, Hao JH (2008) Scr Mater 58:1118
15. Shimuta T, Nakagawara O, Makino T, Arai S (2002) J Appl Phys 91:2290
16. Nakagawara O, Shimuta T, Makino T, Arai S (2000) Appl Phys Lett 77:3257
17. Ortega N, Kumar A, Katiyar RS, Scott JF (2007) Appl Phys Lett 91:102902
18. Zhang JX, Dai JY, Chow CK, Sun CL, Lo VC, Chan HLW (2008) Appl Phys Lett 92:022901
19. Kumar V, Rana A, Yadav MS, Pant RP (2008) J Magn Magn Mater 320:1729
20. Zhang JX, Dai JY, Chan HLW, Phys Rev B (revised)
21. Cullity BD (1972) Introduction to magnetic materials. Addison-Wesley Publishing Company, Reading, MA, p 266
22. Vavassori P, Bonanni V, Busato A, Bisero D, Gubbiotti G, Adeyeye AO, Goolaup S, Singh N, Spezzani C, Sacchi M (2008) J Phys D Appl Phys 41:134014
23. Wu H-C, Arora SK, Mryasov ON, Shvets IV (2008) Appl Phys Lett 92:182502